Journal of Asian Earth Sciences 285 (2025) 106558

Contents lists available at ScienceDirect

Journal of Asian Earth Sciences

journal homepage: www.elsevier.com/locate/jseaes

Full length article

Origin, maturity and geochemistry of natural gas in the Yancheng Sag, Subei Basin, China: Insights from pyrolysis experiments and basin modeling

Yuantao Tang [a,b], Kai Xue [a,b], Xianzhi Gao [a,b,*], Yan Song [a,b], Heyong Li [c], Yonghui Wang [a,b]

[a] National Key Laboratory of Petroleum Resources and Engineering, China University of Petroleum (Beijing), Beijing 102249, China
[b] College of Geosciences, China University of Petroleum (Beijing), Beijing 102249, China
[c] Research Institute of Exploration and Development, SINOPEC Jiangsu Oilfield Company, Jiangsu 225009, China

ARTICLE INFO

Keywords:
Gas-source correlation
Gold tube Pyrolysis
Basin modeling
Subei Basin
Carbon isotopes

ABSTRACT

Natural gas-sources correlation is crucial for determining the target of natural gas accumulation. The Zhujiadun gas field discovered in the Cretaceous Taizhou-Paleogene Funing (K_2t-E_1f) formations is one of the most important gas fields in the Subei Basin. However, the origin of natural gas in the Zhujiadun gas field is controversial, seriously restricting future exploration. In this study, organic geochemistry, gold-tube hydrous pyrolysis experiments, and basin modeling were performed to comprehensively investigate the origin, maturity and geochemistry of natural gas in the Zhujiadun gas field. The results show that: (1) the natural gas in this gas field is sapropelic-sourced thermogenic gas, which is predominately from the secondary cracking of crude oil. (2) New empirical equations for calculating the maturity of natural gas in the Yancheng sag are established based on the relationship between the carbon isotopic composition of methane and the thermal maturity of kerogen. The calculated average Ro value of natural gas is 2.2 %. (3) The Yancheng Sag has evolved through three subsidence cycles. Potential Paleozoic source rocks are currently in the post-maturity period, while the Paleogene source rocks are still in the oil generation window. (4) The natural gas in the Zhujiadun gas field predominantly originates from the source rocks of the Ordovician Wufeng-Silurian Gaojianbian formations. These results provide insights into the source of natural gas in the Zhujiadun gas field and a basis for natural gas exploration in the future.

1. Introduction

Rich in natural gas resources, the Yangtze region is a crucial natural gas exploration area in China. A series of gaseous hydrocarbon-bearing strata have been discovered in the Sichuan Basin in the upper Yangtze area except for the oil-producing Jurassic strata in central Sichuan Basin, which means the Sichuan Basin is a gas-prone petroliferous basin (Li et al., 2019). In contrast, in the Subei Basin, which is located in the lower Yangtze area, commercial oil and gas exploration is mainly conducted in the Mesozoic and Cenozoic strata, and large gas fields have rarely been discovered. Petroleum exploration in the Yancheng Sag of the Subei Basin began in the 1950 s, and the discovery of the Zhujiadun gas field was announced after high-yield natural gas flows were obtained in wells A1 and A3 in 1999 (Li and Zhang, 2017). However, the controversies concerning the source of natural gas seriously restrict natural gas exploration in the K_2t-E_1f formations.

Although it is generally believed that the natural gas in the Zhujiadun gas field originates from the Paleozoic source rocks, the source of the natural gas in the gas field is still controversial due to the possible existence of multiple suites of potential source rocks. Serval possible sources of natural gas have been proposed: (1) the Upper Paleozoic coal-bearing source rocks (Chen et al., 2001); (2) the Upper Paleozoic sapropelic source rocks (Chang et al., 2004); (3) the Lower Paleozoic marine source rocks (Luo et al., 2020; Zhang et al., 2006); (4) the Permian Qixia Formation (Peng et al., 2023; Xu, 2002). These differences regarding the source of natural gas can be attributed to different interpretations of the geochemical characteristics of natural gas in the K_2t-E_1f formations and the thermal maturity of potential source rocks.

Identifying the source of the gas is critical to decoding the process behind gas accumulation, which has important implications for the natural gas industry, and the accurate assessment of maturity is one of fundamental scientific problem in gas-source correlation (Lotfy et al., 2024; Schwangler et al., 2020; Shen et al., 2024;). Numerous pyrolysis experiments and gas data sets for different basins and gas fields have

* Corresponding author at: National Key Laboratory of Petroleum Resources and Engineering, China University of Petroleum (Beijing), Beijing 102249, China.
E-mail address: gaoxz@cup.edu.cn (X. Gao).

https://doi.org/10.1016/j.jseaes.2025.106558
Received 16 May 2024; Received in revised form 7 January 2025; Accepted 10 March 2025
Available online 14 March 2025

been used to assess the effect of maturity on the geochemical characteristics of gaseous hydrocarbons from different types of kerogens in various systems (Behar et al., 1995; Berner and Faber, 1996; Dieckmann et al., 2006; Lorant et al., 1998; Tian et al., 2012; Wang et al., 2013). Based on these, various diagnostic plots and empirical equations have been proposed to evaluate the maturity of natural gas (Bernard et al., 1978; Chen et al., 2021; Dai et al., 1985; Li and Zhang, 2017; Schoell, 1983; Stahl, 1977). Case studies for various basins have demonstrated the applicability and practicability of these empirical plots and equations, but ambiguous conclusions may be encountered when they are applied to complex sedimentary basins with very high maturity (Dai et al., 2024; Gai et al., 2019; Liu et al., 2019; Schoell, 1983; Stahl, 1977). In contrast, the maturity of source rocks can be accurately evaluated using experimental methods. However, the available drilling data for the Yancheng Sag is mainly focused on Mesozoic and Cenozoic strata, making it difficult to accurately determine the current maturity of Paleozoic source rocks. The thermal evolution process of potential Paleozoic source rocks in the study area needs to be clarified because the lack of clarity in respect thereof poses serious restrictions to the research on the genesis and source of natural gas.

In this study, gold-tube hydrous pyrolysis experiments and basin modeling were conducted to minimize the constraints from a complex sag that has been explored to a low extent. Integration of gold-tube hydrous pyrolysis experiments with basin modeling provides insights into the formation of gas pools in the Yancheng Sag, which is a comprehensive attempt for the gas-source correlation. Therefore, the genetic type of natural gas in the Yancheng Sag was determined based on the chemical composition, isotope characteristics, and light hydrocarbons of natural gas. A comparative study was carried out using the gas from gold-tube hydrous pyrolysis experiments and kerogen to further analyze the maturity of natural gas. In addition, basin modeling was performed to reconstruct the thermal evolution history of potential source rocks. The main source of natural gas in the K_2t-E_1f formations was determined by analyzing the differences in genesis, maturity, and carbon isotopic composition between natural gas and source rocks. The results provide an essential basis for better understanding natural gas accumulation in the Yancheng Sag, valuable information for further exploration of marine shale gas of the Yancheng Sag, and a practical reference for other similar regions characterized by low extent of exploration.

2. Geological setting

Located in Southern China, the Yangtze region covers an area of approximately 12.01 × 10^4 km^2 and is connected to the North China Block by the Qinling-Dabie orogenic belt (Zhang et al., 2018), bordering the west rim of the circum-Pacific orogenic belt in the east, the Sanjiang orogenic belt in the west, and the Xuefeng-Jiangshao orogenic belt in the south (Fig. 1a). Complete Sinian-Cenozoic stratigraphic sequences have developed in the Yangtze region, and marine shales mainly exist in the Paleozoic strata (Liang et al., 2014; Zou et al., 2010). Serval large gas fields have been discovered in the marine stratigraphic sequences in the Sichuan Basin, such as Weiyuan, Puguang and Yuanba, (Korsch et al., 1991; Li et al., 2016, 2015; Ma et al., 2007). The Yangtze Block can be divided into three sub-blocks, namely, upper, middle, and lower Yangtze areas (Gong et al., 2022). Located in the lower Yangtze area, the Subei Basin is a rift basin that began to form at the western border of the Yellow Sea during the Late Cretaceous (Quaye et al., 2019), bounded by the Tanlu fracture zone in the west, the Sulu orogenic belt in the north, and the Sunan uplift in the south (Fig. 1a). There have been two major stages of rifting activities thereafter accompanied by rapid subsidence (Liu et al., 2021; Quaye et al., 2019).

The Yancheng Sag is a dustpan-shaped sag located in the Yanfu Depression in the northeastern part of the Subei Basin, covering an area of approximately 2.1 × 10^3 km^2. A series of tectonic events including the Yizheng, Wubao, Sanduo and Yancheng Movements occurred throughout the evolutionary process of the Yancheng Sag. In the late Cretaceous, the Yizheng Movement activated the faults that controlled sediment deposition in the sag, forming the prototype of the present-day structural pattern. The strong regional uplift triggered by the Sanduo Movement resulted in extensive erosion during the Oligocene (Chen, 2009). The Paleozoic strata underwent several periods of intense extrusion-induced deformation and tension-induced deformation, during which a thrust complex model was formed below the Cretaceous Pukou formation (Zhu and Meng, 2004). The Yancheng Sag is divided from north to south into three secondary units, namely, the Xinyang sub-sag, the central uplift fault zone, and the Nanyang sub-sag (Fig. 1b). Almost all of the drilled wells with commercial gas flows are located between the Yan2 and Yan3 faults in the southern part of the Yancheng Sag.

In terms of stratigraphy, there are several formations of potential source rocks in the lower Yangtze area, including the Lower Cambrian Mufushan formation (ϵ_1m), the Ordovician Wufeng-Silurian Gaojianbian formations (O_3w-S_1g), the Permian formations, the Cretaceous Taizhou (K_2t), and the second member of the Paleocene Funing formation (E_1f^2) from bottom to top (Fig. 2). The Permian formations consists of the Qixia (P_1q), Gufeng (P_2g), Longtan (P_3l) and Dalong (P_3d) formations. The source rocks in P_2g and P_3d are mainly mudstone and dark shale, and the dominant type of source rock in P_1q is gray limestone intercalated with argillaceous deposits. The source rocks in P_3l are marine-continental transitional facies that are composed primarily of sandstone, mudstone, and coal beds. As platform sediment, the source rock of ϵ_1m is dominated by shale, and it is regional source rock with great hydrocarbon generation potential in the Yangtze region that has

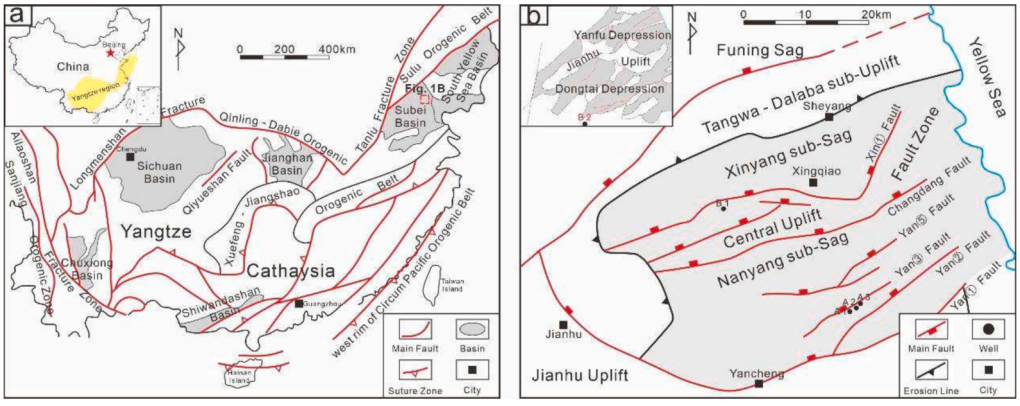

Fig. 1. (a) Geographical location and structural map of the Yangtze region (modified after Cai et al., 2019); (b) Distribution of structural units and wells in the Yancheng Sag.

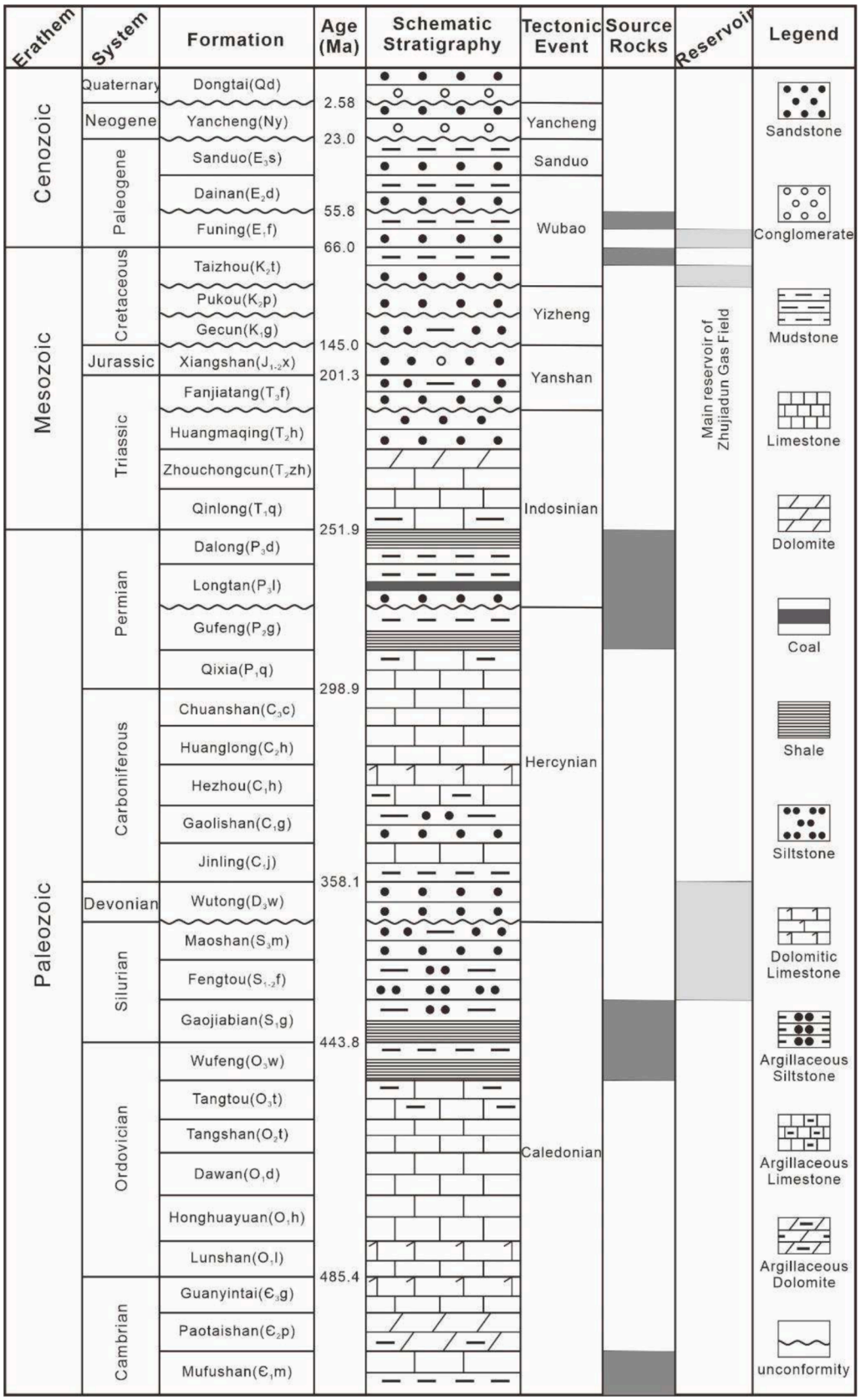

Fig. 2. Generalized stratigraphic column of the Paleozoic-Cenozoic strata (modified after Peng et al., 2023).

made great contributions to Weiyuan gas fields (Liang et al., 2017). The lower Yangtze area was a semi-closed sea basin situated in a reducing sedimentary environment during the period from the Late Ordovician to the Early Silurian, where black shale and aragonitic siltstone were deposited, forming the O_3w-S_1g formations (Li et al., 2023). The organic-rich shales of these formations share similar characteristics with those of the Ordovician-Silurian strata in the upper Yangtze area (Li et al., 2023).

3. Samples and methods

3.1. Samples

Two representative mudstone samples were collected at the Permian Longtan Formation and the Ordovician Wufeng Formation from Well B1 and Well B2 in the lower Yangtze area to determine the relationship between maturity and carbon isotopes of gaseous products. Gold-tube hydrous pyrolysis experiments were conducted to identify the source and maturity level of natural gas. Each sample was ground into 100-mesh powder and extracted to minimize the interference of residual hydrocarbons. Geochemical information about the representative mudstone sample is showed in Table 1.

Numerous natural gas samples collected by Sinopec Jiangsu Oilfield Company from the E_1f_1 and K_2t formations in the Yancheng Sag were tested for the purpose of identifying their components and analyzing stable carbon isotopes. These samples were collected directly from continuous gas flows at wellheads using double-valve high-pressure steel cylinders for protection against contamination, and the cylinders were subsequently immersed in water for leak testing. The geochemical analysis of most samples was carried out at Sinopec Key Laboratory of Petroleum Accumulation Mechanisms (Wuxi) and Petroleum Exploration and Production Research Institute of Sinopec Jiangsu Oilfield Company.

3.2. Methods

3.2.1. Gold-tube hydrous pyrolysis experiments

Pyrolysis experiments were conducted in an ST-120- II gold-tube thermal simulation apparatus at the State Key Laboratory of Petroleum Resources and Prospecting with a sealed gold tube under hydrous conditions. First, a PUK U4 argon-arc welder with microscope (Lampert Werktechnik) was used for welding at one end of the gold tube with a length of 60 mm, an inner diameter of 5.5 mm, and a wall thickness of 0.25 mm (Wu et al., 2021). After cooling to room temperature, proper amounts of extracted sample and distilled water were packed into the gold tube. The gold tube was purged with argon for five minutes to displace the air in the tube before crimping and welding the open end, and then the tube was loaded into a stainless-steel autoclave. Subsequently, the tube was gradually heated to the predetermined temperatures. The hydrocarbon generation process was simulated at eight different temperatures ranging from 280 °C to 560 °C at a constant interval of 40 °C. For each autoclave, the internal pressure was maintained at 50 MPa, and the gold tube inside the autoclave was heated for 72 h at each preset temperature. After cooling, the gold tube was punctured with a needle for sampling. Vitrinite reflectance analysis was performed on the residual powder in the gold tube, and the gaseous hydrocarbons obtained at each temperature were collected and tested to identify their components and carbon isotope characteristics.

3.2.2. Isotopic analysis and vitrinite reflectance (Ro) analysis

Gas sample components were identified using an Agilent 8890 GC equipped with a flame ionization detector and a thermal conductivity detector. Individual gaseous hydrocarbon components were separated using an Agilent 19091P capillary column (length: 27 m, inner diameter: 0.32 mm, film thickness: 8 μm). The temperature of the Agilent 8890 GC was first set to 50 °C, which was held for 1 min, then increased to 80 °C at a rate of 20 °C /min, and finally ramped up to 190 °C at a rate of 30 °C /min with a hold of 7 min. Stable carbon isotopes were detected with a MAT 253 IRMS. High-purity helium was served as the carrier gas at a flow rate of 1.3 mL/min. The temperature was initially programmed at 40 °C for 5 min, then increased to 85 °C at a rate of 15 °C/min, and finally ramped up to 250 °C at a rate of 8 °C/min with a 5 min hold. The mass spectrometer has an electron ionization detector (EI), and electronic energy of 70 eV. The tests were completed in the National State Key Laboratory of Petroleum Resources and Engineering, China University of Petroleum (Beijing).

A Leica DM4500P microscope equipped with a CRAIC photometer and a 50 × oil immersion objective was used to measure the mean random reflectance values. The solid samples were ground, solidified with epoxy resin, sliced into sections, and finally polished using a polishing machine. Since vitrinite is absent in samples, bitumen reflectance (BRo) in sedimentary rocks is often used as a proxy for maturity (Hackley et al., 2024; Schmidt et al., 2019). The results of thermal simulation experiments have demonstrated that solid bitumen is sensitive to temperature, with its reflectance increases as temperature rises, indicating that increasing BRo serves as a reliable indicator of organic matter maturity and thermal evolution in shales (Hackley et al., 2024; Luo et al., 2025). Indeed, numerous factors can influence bitumen reflectance, including lithology, the type of solid bitumen, optical properties of solid bitumen, the porosity development within solid bitumen, and the original kerogen composition (Luo et al., 2025). These variables can impose limitations on the reliability of BRo as a sole indicator of thermal maturity. To mitigate the impact of these factors and enhance the accuracy of maturity assessments, it is essential to measure the reflectance of solid bitumen that is uniformly distributed and compositionally similar. However, the use of the reflectance of solid bitumen as a thermal maturity indicator is not compatible with other thermal maturity proxies (Mastalerz et al., 2018). Therefore, the bitumen reflectance data was converted to equivalent vitrinite reflectance values using the following regression equation: $EqVRo = 0.938\ BRo + 0.3145$ (Schmidt et al., 2019).

3.2.3. Basin modeling

Reconstructing the burial-thermal evolution history of the Yancheng Sag is beneficial for clearly understanding the deposition and hydrocarbon generation processes of Paleozoic source rock. For this purpose, the PetroMod 2014 software was used for 1D modeling. The required input data set in the PetroBuilder module contains data concerning volumetric lithological mixes, thicknesses of the present-day strata, ages of geological units, erosion, sediment–water interface temperature (SWIT), and heat flow (HF) (Farouk et al., 2024a, 2024b). The HF values were mainly referenced from Well B2 (Yuan et al., 2016), with slight modifications based on measured Ro values. The detailed variations are

Table 1
Analyzed data of TOC and Rock-Eval pyrolysis about the representative mudstone samples.

Sample	Well	Depth (m)	Formation	Kerogen type	TOC	S_1	S_2	Tmax	Ro
Sample 1	B1	2703.63	O_3w	type II	1.33	0.49	2.74	442	0.94
Sample 2	B2	2076.82	P_3l	type III	4.87	0.92	2.17	465	1.46

Note: TOC: total organic carbon, wt%; S_1: residual hydrocarbon, mg HC/g rock; S_2: pyrolysis hydrocarbon, mg HC/g rock; Tmax: peak temperature of pyrolysis, °C; Ro: vitrinite reflectance, %Ro.

shown in Fig. 3a. The SWIT value was derived from the global mean surface temperature (GMST) map made by Wygrala (1989), which was automatically calculated by picking up the latitude of the study area. The latitude of the Yancheng Sag is 33 degrees (North Latitude, East Asia), and its SWIT value ranges from 18.8 °C to 20 °C, as suggested by Wygrala (1989) (Fig. 3b). The dominant lithology, present stratigraphic thickness, and erosion in the Yancheng Sag were determined based on the internal reports provided by Jiangsu Oilfield Company and previously published data of the South Yellow Sea Basin and the lower Yangtze area (e.g., Cai et al., 2019; Du et al., 2020).

In order to calibrate the model with the vitrinite reflectance data provided by Jiangsu Oilfield Company, the parameter HF was adjusted because the vitrinite reflectance data used as a maturity indicator is closely related to the paleo-heat flow. Furthermore, to effectively simulate the thermal maturation process of Paleozoic source rocks, the chemical kinetic easy %Ro routine developed by Sweeney and Burnham (1990) was employed. However, the available Ro data for the Paleozoic strata in the Yancheng Sag is limited. Source rock strata older than the Mesozoic strata have been encountered only in Well B1, which was drilled into the Ordovician Wufeng Formation in the uplift zone. Because no wells have been drilled to the Paleozoic source rocks in the depression, Paleozoic rock samples with high maturity are unavailable, resulting in the lack of Ro data. Therefore, the empirical equation representing the relationship between depth and Ro provided by Jiangsu Oilfield Company was employed to calculate the Ro values of strata at 6000 m and greater depths, and it was used in conjunction with the measured Ro values from shallower strata to calibrate the thermal evolution history. As shown in Fig. 3c, the measured and calculated values of Ro are highly consistent with the results from the kinetic model (Easy% Ro) of Sweeney and Burnham (1990), where the dark gray circles represent measured Ro values, and the light gray triangles represent calculated Ro values.

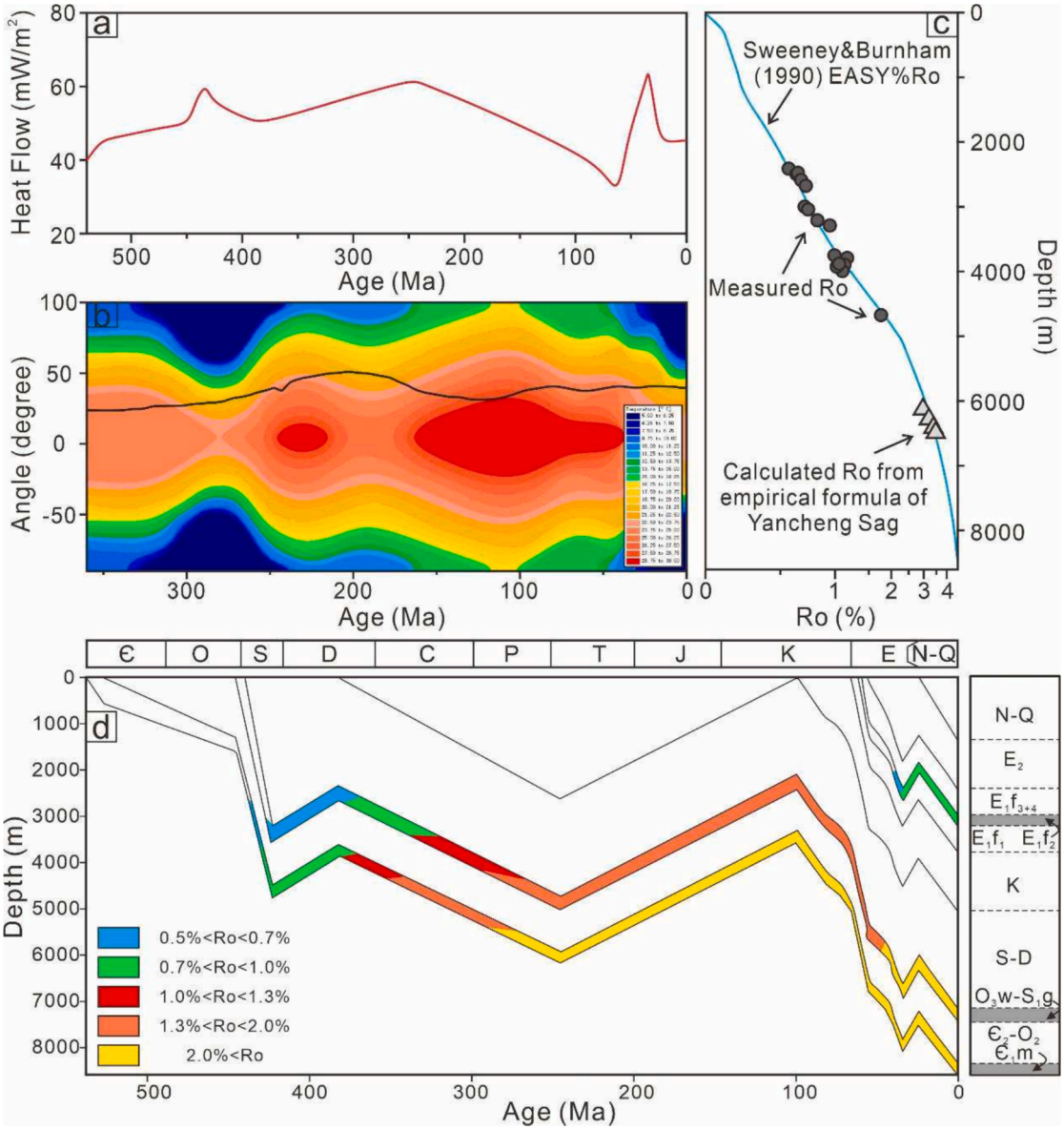

Fig. 3. Boundary conditions and calibration for the basin modeling of the Yancheng Sag. (a) Heat flow trend assigned to the model; (b) GMST map based on Wygrala (1989); (c) Calibration of Ro; (d) Burial and thermal evolution history of the pseudo-well in the Yancheng Sag, Subei Basin. Ny: Neogene Yancheng Formation; E_2s: Paleocene Sanduo Formation; E_2d: Paleocene Dainan Formation; E_1f_4: The fourth member of the Paleocene Funing Formation; E_1f_3: The third member of the Paleocene Funing Formation; E_1f_2: The second member of the Paleocene Funing Formation; E_1f_1: The first member of the Paleocene Funing Formation; O_3w-S_1g: Ordovician Wufeng-Silurian Gaojianbian formations; $Є_2$-O_2: Middle Cambrian- Middle Ordovician formations; $Є_1$m: Cambrian Mufushan Formation.

4. Results

4.1. Natural gas composition

Methane were the major components of the natural gas samples obtained from the K_2t-E_1f formations, and the content of most samples is greater than 90 %, except for two samples whose content is lower than 90 % (Table 2). The heavy alkane gas content is very low and the butane content is undetectable in nearly half of the samples. The dryness coefficients of all natural gas samples were all above 0.95, indicating the characteristics of dry gases (Farouk et al., 2024c). This suggests that natural gas accumulated in the K_2t-E_1f formations in the Yancheng Sag has a high degree of thermal maturity. The natural gas samples from the Yancheng Sag have low CO_2 content ranging from 0.57 % to 10.05 %.

4.2. Gaseous hydrocarbon maturity in pyrolysis experiments

The measured Ro values for the heated mudstone and the corresponding calculated EASY%Ro according to Sweeney and Burnham, 1990 are listed in Table 3. For Sample 1 within Wufeng Formation, the measured Ro values are generally similar to the calculated EASY%Ro values at EASY%Ro < 2.5. At higher maturities, the gap between measured Ro values and calculated EASY%Ro values gradually increase. For Sample 2 within Longtan Formation, the measured Ro values are much higher than the calculated EASY%Ro values at EASY%Ro < 2.5, then increasingly lower than EASY%Ro values at higher maturities, with trend similar to Sample 1. The thermal properties are contingent upon the variability in kerogen type, as well as the hydrogen index, which collectively regulate the physical and chemical transformation of organic matter. To minimize uncertainty, the maturity of the gaseous hydrocarbon is assessed using vitrinite reflectance of residual kerogen from gold tube pyrolysis experiments, providing a reliable basis for determining the source of natural gas in the Yancheng Sag.

4.3. Carbon isotopes of natural gas

Carbon isotopic composition of natural gas can reflect the genetic type of natural gas. Generally, the carbon isotopic composition of gaseous hydrocarbons may be a normal order series ($\delta^{13}C_1 < \delta^{13}C_2 < \delta^{13}C_3 < \delta^{13}C_4$), a partially reversed order series (e.g., $\delta^{13}C_1 > \delta^{13}C_2 < \delta^{13}C_3 < \delta^{13}C_4$), or a wholly reversed order series ($\delta^{13}C_1 > \delta^{13}C_2 > \delta^{13}C_3 > \delta^{13}C_4$). Carbon isotope reversals can be caused by different factors related to thermal effects (Berner and Faber, 1988; Dai et al., 2004; James, 1990; James and Burns, 1984). Gaseous hydrocarbons with a regular carbon-isotope order are typically of organic origin. The average carbon isotopes of methane, ethane, butane, and propane in natural gas samples from the Yancheng Sag are −38.14 ‰, −27.39 ‰, −25.22 ‰, and −24.64 ‰, respectively. This positive trend is the same as the result of Peng et al. (2023), indicating that the natural gas in the Yancheng Sag is of organic origin and comes from a single source.

The carbon isotope values of gaseous hydrocarbons in the pyrolysis experiment are listed in Table3. There is a good correlation between $\delta^{13}C_1$ values and temperature, and the carbon isotope values typically tend to rise as the simulated temperature increases. However, $\delta^{13}C_1$ inversion ($\delta^{13}C_1$ values become lighter as the degree of maturity increases) occurs in the early stage of thermal simulation of hydrocarbon generation, as observed in many closed-system and open-system pyrolysis experiments (Berner et al., 1995; Dieckmann et al., 2006; Tian et al., 2012; Wang et al., 2013). Numerous studies have attempted to account for this phenomenon, which can be summarized as follows: (1) disproportionation reactions during pyrolysis experiments (Xiong et al., 2004; Zhang et al., 2005); (2) structural complexity and heterogeneity of organic matter (Shuai et al., 2003; Lu et al., 2019); (3) complex precursors in immature or low-maturity kerogen (Hill et al., 2003; Lorant et al., 1998); (4) separation of heteroatomic functional groups (He et al., 2018); and (5) isotopic fractionation (Tang et al., 2000). The variations of methane carbon isotopes show a two-stage distribution (Fig. 4). When Ro > 1.2 %, methane carbon isotopes are linearly correlated with Ro and increase as the degree of thermal maturity increases. As organic matter matures, further cracking of kerogen and liquid hydrocarbons occurs, and methane becomes progressively isotopically heavier. The following empirical equations for oil-derived gas and coal-derived gas were established based on gold-tube pyrolysis experiments:

$$Coalderivedgas: \delta^{13}C_1 = 7.0697 \times Ro - 47.453 (R^2 = 0.932) \quad (1)$$

$$Oilderivedgas: \delta^{13}C_1 = 4.6693 \times Ro - 48.208 (R^2 = 0.971) \quad (2)$$

Where $\delta^{13}C_1$ is methane carbon isotopes, Ro represents the maturity of natural gas, and the constants are fitted with the data obtained from thermal simulation experiments.

4.4. Burial and thermal maturity history of source rocks

In order to reconstruct the thermal maturation history of Paleozoic source rocks, a pseudo-well was created in the Zhujiadun area, Yancheng Sag. The pseudo-well represents a combination of shallow strata data from Well A1 and deep strata data from seismic data when well data is not available. Based on well data and seismic data, the thermal evolution process of the primary source rocks in the Zhujiadun gas field was simulated. The reconstructed burial and thermal maturation history of the pseudo-well is shown in Fig. 3d. The burial history reveals a process of steady subsidence and sedimentation in the study area for the majority of the Paleozoic and Cenozoic and strong uplift during the Mesozoic. It is to be noted that the reburial process during the Neogene–Quaternary period did not result in any desired spike in the thermal maturity of source rocks because the formation temperature during reburial did not exceed the previously experienced maximum temperature. Consequently, the maturity of each suite of source rocks remained constant as the formation temperature dropped since the Late Oligocene.

Table 2
Molecular composition and stable carbon isotopic compositions of gas samples from K_2t-E_1f in the Yancheng Sag.

Gas Sample No.	Formation	Gas compositions (%)								δ13C (‰, PDB)				
		CH_4	C_2H_6	C_3H_8	iC_4H_{10}	nC_4H_{10}	iC_5H_{12}	nC_5H_{12}	CO_2	$\delta^{13}C_1$‰	$\delta^{13}C_2$‰	$\delta^{13}C_3$‰	$\delta^{13}C_4$‰	$\delta^{13}CO_2$‰
1	K_2t-E_1f	61.90	0.72	0.40	0.03	0.04			3.30	−38.50	−28.30			−13.60
2	K_2t-E_1f	64.46	1.46	0.65	0.18	0.14	0.09	0.08	10.05	−39.60	−27.20		−28.20	−15.80
3	K_2t-E_1f	93.96	2.83							−38.10	−26.60			
4	K_2t-E_1f	92.20	2.91	0.79	0.27	0.16	0.05	0.04	0.83	−38.38	−27.58	−25.47	−24.80	−15.52
5	K_2t-E_1f	96.57	1.56	0.34	0.07	0.08	0.03	0.02		−37.80	−27.66	−25.83	−25.40	
6	K_2t-E_1f	94.35	3.17	0.26	0.05	0.05	0.01		0.57	−37.95	−27.28	−25.33	−25.13	−25.50
7	K_2t-E_1f	90.82	1.00	0.07						−36.70	−27.10			
8	K_2t-E_1f	96.51	1.71	0.38	0.12	0.08			1.20	−37.80	−28.10	−25.30	−24.40	−13.80
9	K_2t-E_1f	92.77	2.38	0.65	0.23	0.18	0.11	0.10	1.26	−38.40	−26.70	−24.21	−23.45	−9.30

Table 3
Information about mudstone samples in pyrolysis experiment.

		320°C	360°C	400°C	440°C	480°C	520°C	560°C
EASY%Ro		0.82	1.2	1.75	2.46	3.27	3.96	4.45
Measured Ro	Sample 1	0.95	1.31	1.6	2.24	2.59	3.08	3.4
	Sample 2	1.5	1.62	1.89	2.49	2.66	3.22	3.72
$\delta^{13}C_1$/‰	Sample 1	−33.4	−40.7	−40.9	−38.1	−35.6	−33.8	−32.0
	Sample 2	−30.5	−37.1	−35.9	−30.7	−27.9	−26.2	−30.0

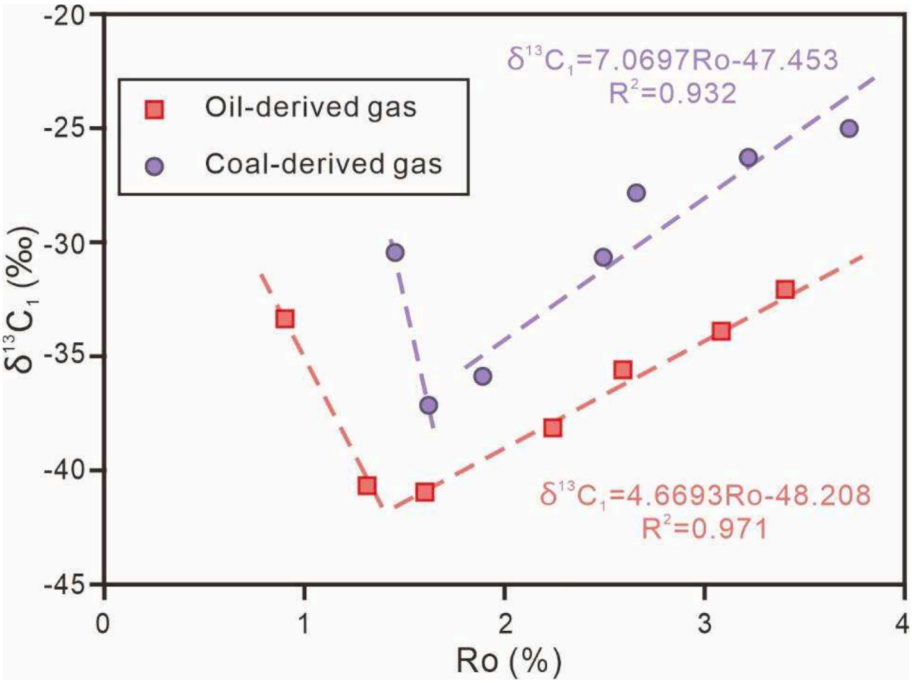

Fig. 4. Relationship between $\delta^{13}C_1$ and Ro for oil-derived gas and coal-derived gas during the gold-tube pyrolysis experiment.

5. Discussion

5.1. Genetic types of natural gas

Molecular composition and carbon isotopes were extensively utilized to ascertain the genetic types of natural gas, and many discriminants chart crafted from rigorous data analysis has effectively facilitated the identification of natural gas origins (Hu et al., 2010; Li and Zhang, 2017; Lorant et al. 1998; Odden et al., 1998; Schoell 1983).

The compositional analysis of light hydrocarbons provides a valuable approach to determining the genetic types of natural gas (Huang et al., 2022). The parameters in commonly used ternary diagrams include nC_7, various structures of dimethyl cyclopentane ($DMCC_5$), and methylcyclohexane (MCC_6) (Hu et al., 2010; Odden et al., 1998). Due to the distinct origins of the three elements in the nC_7-$DMCC_5$-MCC_6 ternary diagram, it is possible to differentiate between sapropelic type and humic type natural gas. Fig. 5a shows the relative abundance of *n*-heptane in light hydrocarbons, which indicates that the gas in the K_2t-E_1f formations primarily originates from sapropelic kerogen. The combination of C_5-C_7 *n*-alkanes, *iso*-alkanes, and cycloalkanes is also helpful in determining the genetic types of natural gas (Hu et al., 2008). All natural gas samples falling within the category of sapropelic type gas indicates

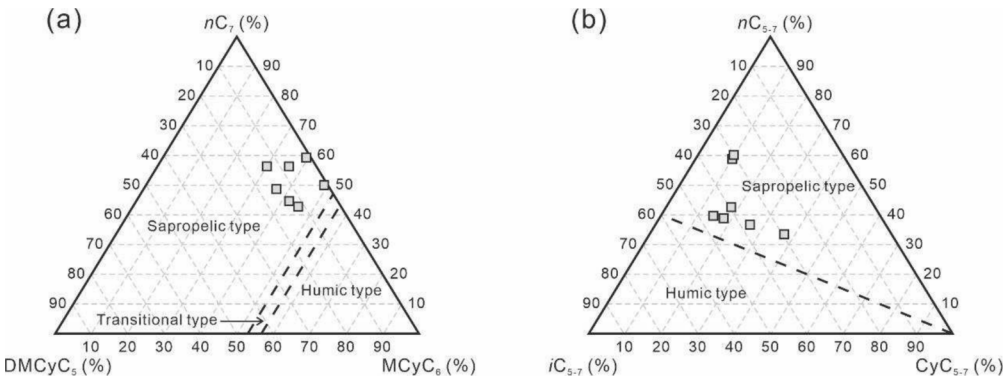

Fig. 5. Diagrams of C_5-C_7 light hydrocarbons in natural gas from the Yancheng Sag. (a) Ternary diagram of $nC_{5\text{-}7}$-$iC_{5\text{-}7}$-$CyC_{5\text{-}7}$; (b) Ternary diagram of nC_7-$DMCC_5$-MCC_6.

that the primary source of natural gas in the K_2t-E_1f formations is sapropelic kerogen (Fig. 5b).

Isotopic differences can be used to distinguish between thermogenic and microbial gases. Fig. 6a indicates that the gas samples from K_2t-E_1f are thermogenic in origin, with limited variation in the $C_1/(C_2 + C_3)$ ratio and $\delta^{13}C_1$ value. Based on an extensive data analysis, Schoell (1983) proposed a diagram of methane carbon isotopes versus ethane carbon isotopes to distinguish between sapropelic type and humic type

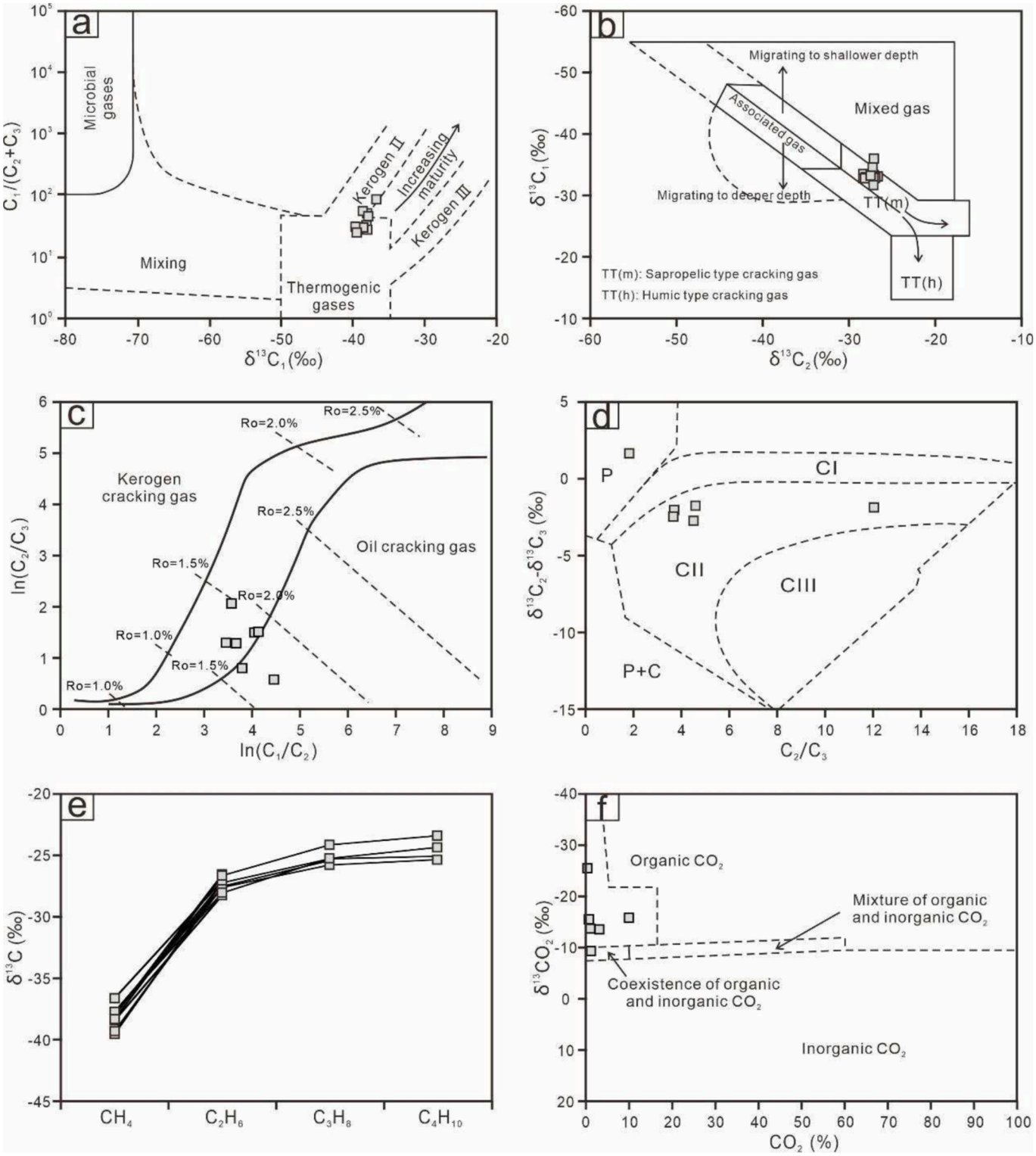

Fig. 6. Diagram for the identification of origin and geochemistry based on gas components and carbon isotopes. (a) Plot of $C_1/(C_2 + C_3)$ versus $\delta^{13}C_1$ (modified after Bernard et al., 1978); (b) Plot of $\delta^{13}C_1$ versus $\delta^{13}C_2$ (modified after Schoell, 1983); (c) Diagram of $\ln(C_1/C_2)$ versus $\ln(C_2/C_3)$, (modified after Li and Zhang, 2017); (d) Diagram of C_2/C_3 versus $\delta^{13}C_2$-$\delta^{13}C_3$ (modified after Lorant et al., 1998). P: primary cracking; CI: secondary cracking of oil; CII: secondary cracking of oil and gas; CIII: secondary cracking of gas; P + C: mixture of primary cracking and secondary cracking of oil; (e) Distribution characteristics of the carbon isotopes of methane, ethane, butane, and propane in natural gas; (f) Genetic discriminant diagram of $\delta^{13}CO_2$ versus CO_2 content in natural gas (modified after Dai et al., 2017).

gases. The data points for gas samples from K_2t-E_1f are concentrated in the irregular part of the $\delta^{13}C_1$-$\delta^{13}C_2$ diagram (Fig. 6b), representing gas from thermal cracking of sapropelic kerogens.

However, oil-derived gas can originate from the cracking of organic matter or secondary cracking of crude oil (Behar et al., 1995; Lotfy et al., 2022; Prinzhofer et al., 2000). The diagram of $\ln(C_1/C_2)$ and $\ln(C_2/C_3)$ has been widely used to distinguish between kerogen cracking gas and oil cracking gas (Li and Zhang, 2017). Fig. 6c shows that the data points for the gas samples fall between the lines representing kerogen cracking gas and oil cracking gas and are close to the right edge, indicating that the natural gas in K_2t-E_1f consists primarily of oil cracking gas. The kinetic model for gaseous hydrocarbon generation and degradation proposed by Lorant et al. (1998) provides a new understanding of the genetic processes of gaseous hydrocarbons. To be precise, the process of gas production from the cracking of hydrocarbon molecules or kerogen corresponds to different stages of thermal evolution. As the degree of cracking increases, the C_2/C_3 ratio increases, and the $\delta^{13}C_2$-$\delta^{13}C_3$ values decrease. Most of the gas samples are characterized by a narrow range of $\delta^{13}C_2$-$\delta^{13}C_3$ values and a broad range of C_2/C_3 values in Region CII, except for one data point that falls in Region P, indicating that the gas samples are composed predominantly of gas from crude oil cracking, with a small amount of gas from kerogen cracking (Fig. 6d).

In addition, the cracking of $C_{2\text{-}5}$ gaseous hydrocarbons (e.g., ethane to methane) typically leads to an increase in $\delta^{13}C_2$, and a sharp increase in carbon isotopes from $\delta^{13}C_1$ to $\delta^{13}C_2$ can be inferred as an indication of ethane cracking (Li et al., 2022). The distribution of carbon isotopes suggests a contribution of natural gas from the cracking of $C_{2\text{-}5}$ gaseous hydrocarbons at the high-maturity stage, which is also verified by the C_2/C_3 versus $\delta^{13}C_2$-$\delta^{13}C_3$ diagram (Fig. 5d and 5e). The $\delta^{13}CO_2$-CO_2 scatter plot developed by Dai et al. (1996) identifies the CO_2 in the Yancheng Sag as an organic gas, suggesting that the gas reservoir contains organic CO_2 and organic hydrocarbon gas (Fig. 6f).

5.2. Maturity of natural gas

Maturity is an important determinant of the carbon isotopic characteristics of natural gas under geological conditions. As the degree of thermal maturity of a hydrocarbon gas increases, the carbon isotopes of the hydrocarbon gas become heavier. Since vitrinite reflectance is generally a good indicator of maturity, it can be assumed that carbon isotopes increase as the value of vitrinite reflectance increases. Several empirical equations have been developed to evaluate the thermal maturity of natural gas based on the linear correlation between$\delta^{13}C_1$ and log (Ro) (Dai et al., 1985; Schoell, 1983; Stahl, 1977).However, these relationships were established based on natural gas samples from different basins involving different sources and accumulation conditions, meaning that natural gas from source rocks in different areas with the same type of organic matter may carry different carbon isotopic signatures. The relationship between carbon isotopes and Ro of natural gas in the Yancheng Sag was constructed based on the gaseous hydrocarbons and residual kerogen from the gold-tube pyrolysis experiment to minimize uncertainty and provide a reliable basis for determining the source of natural gas in the Yancheng Sag. Although the conditions set for thermal simulation experiments on hydrocarbon generation are different from the natural geological conditions, the carbon isotopes of the products from thermal simulation experiments can still be used reliably to perform gas-source correlation (Chen et al., 2008b).

Empirical equations between the carbon isotopes of gaseous hydrocarbons from pyrolysis experiments and Ro can facilitate the maturity level characterization and genesis analysis of natural gas in the Yancheng Sag. Since the natural gas of K_2t-E_1f in the Yancheng Sag was identified as oil-derived gas through a comprehensive analysis of light hydrocarbons, isotopic composition and gas components, Ro was calculated using Eq. (2). The $\delta^{13}C_1$ values range from −39.6 ‰ to −36.7 ‰, and the corresponding Ro values range between 1.84 % and 2.46 %, with an average of 2.2 % (Fig. 7). Ro > 2.0 % means that the organic matter has entered an over-maturity stage, and early liquid hydrocarbons and wet gas will be further cracked, finally producing methane (Tissot and Welte, 1978). This can be corroborated by analyzing the genetic types of natural gas, indicating that the natural gas in K_2t-E_1f is mainly produced from secondary cracking of oil and gas.

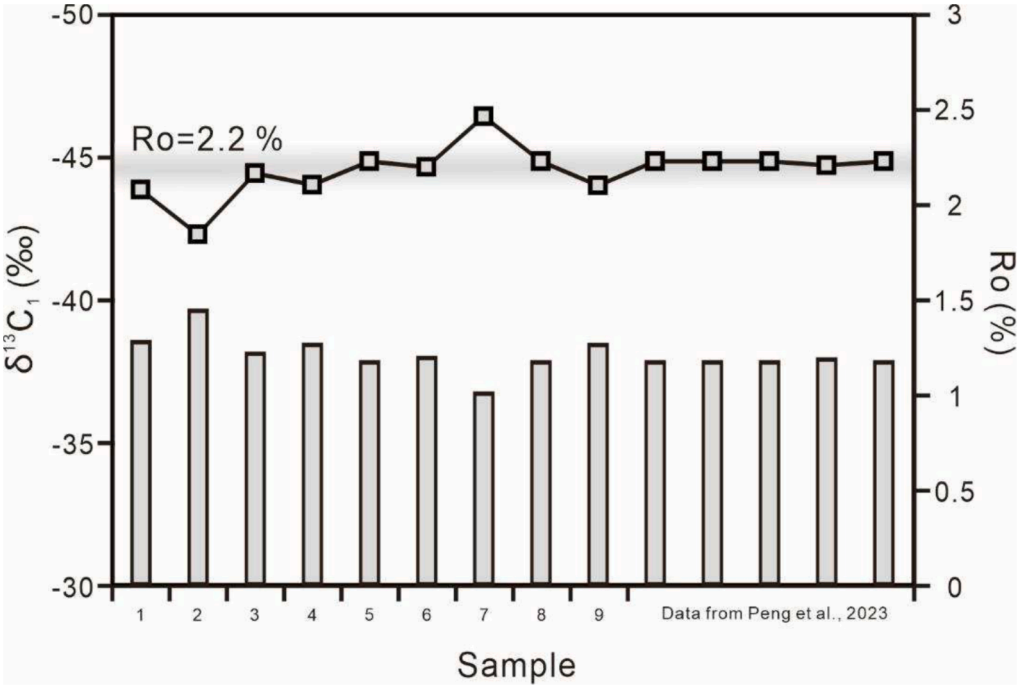

Fig. 7. Distribution characteristics of $\delta^{13}C_1$ and Ro for natural gas samples from the Yancheng Sag. Ro was calculated using the fitting formula of oil-derived gas in the Yancheng Sag. The gray horizontal line represents the Ro value, which is around 2.2%.

5.3. Thermal maturation history of potential source rocks

The shales of the K_2t and E_1f formations are important source rocks in the Subei Basin, which are mature to high mature, with Ro values ranging from 0.5 % to 1.3 % (Gao et al., 2018; Wang et al., 2019). Since the Late Paleocene, all these source rocks have experienced rapid subsidence, sedimentary infilling, and rapid uplift associated with the Wubao tectonic event (Su et al., 2022). The source rock in the second member of E_1f entered the oil generation window in the Eocene and is currently in the medium-maturity stage. In contrast, only the source rock in the lower part of the fourth member of E_1f reached the oil generation threshold before the occurrence of rapid uplift, and its thermal maturity is still low due to the low sedimentation rate. In addition, the source rock of K_2t entered the oil generation window in the Early Paleocene, and oil generation by such source rock has reached its peak.

The Permian source rocks, which are widely distributed in the Yangtze region, have received increasing attention in Southern China in recent years (Wu et al., 2020b). However, the Upper Paleozoic strata in the Yancheng Sag have undergone differential denudation, and the number of wells that can provide information about the distribution of residual strata is limited, resulting in a lack of available Permian samples in the Zhujiadun area. However, the geochemical analysis of samples from the lower Yangtze area indicates that the Permian source rocks are currently in the post-maturity stage (Du et al., 2015, 2020; Zhang et al., 2018).

As one of the primary sources of gaseous hydrocarbons, the source rocks of O_3w-S_1g are widely distributed throughout the Yangtze region. The modeling of the thermal maturation process of these source rocks suggests that such rocks were rapidly buried before the Devonian and reached the hydrocarbon generation threshold in approximately 426 Ma under conditions of steady subsidence and sedimentation. The decrease in formation temperature resulting from the denudation of upper Silurian and middle-lower Devonian sediments slowed down the thermal maturation of source rocks. After the Late Devonian, the continuous burial process further promoted the thermal evolution of source rocks, and the source-rock interval entered the high-maturity stage (Ro = 1.42 %) at the end of the Permian period. The variation of thermal maturation characteristics was limited for the majority of the Mesozoic. This interval entered the dry gas stage in the Early Paleogene, and its maturity remained at a steady level (Ro = 3.8 %) after the Late Oligocene.

According to the results of 1D basin modeling, initial hydrocarbon generation of the source rock of ϵ_1m occurred in the Early Silurian. In the Late Silurian, the Caledonian Orogeny (Guangxi event) led to uplift and erosion of the Lower Yangtze block as a whole (Liang et al., 2017), resulting in reduced heat flow and geothermal gradient (Fig. 3a). These tectonic processes substantially decelerated and even prevented hydrocarbon generation. As the burial and the degree of thermal maturity increased, the source rocks of the Mufushan Formation experienced the transition from peak oil generation to peak gas generation in the Late Paleozoic and then entered the over-maturity stage, and their Ro value reached 2.3 % at the end of the Permian period. Oil-cracking gas and oil-associated gas are gaseous hydrocarbons produced in this period, which exhibit significant isotopic variations. When buried to the maximum temperature in the Late Eocene, the maturity of the source rock has been determined, having a Ro of 4.5 %. The solid bitumen reflectance values of ϵ_1m in Well XY1 are around 5.0 % (Zhao et al., 2021), and the equivalent vitrinite reflectance values are slightly lower because solid bitumen reflectance is lower than vitrinite reflectance unless VR $\geq$ 4.5 % (Schmidt et al., 2019). The slight difference in maturity between the measured data from the lower Yangtze area and the simulation results for the Yancheng Sag indicates that the thermal model of the pseudo-well in the Yancheng Sag is reliable.

5.4. Gas-source correlation

The thick organic-rich shales of the second and fourth members of E_1f, which are widely distributed in the Subei Basin, were deposited in semi-deep to deep lacustrine environments. Because these shales are currently in the early to peak stage of oil generation, their main products are liquid hydrocarbons. Therefore, E_1f is an excellent target for shale oil exploration (Su et al., 2022). However, the isoheptane values of light hydrocarbons in the study area range from 3 to 8 (Luo et al., 2020), indicating a high-maturity (thermal evolution) stage that doesn't match the maturity level of source rocks in E_1f. In addition, the carbon isotopes of kerogen are more depleted than those observed in ethane (Fig. 8). Therefore, the inconsistencies in carbon isotopic composition and maturity between natural gas and kerogen in E_1f reveal that the natural gas in K_2t-E_1f is unlikely to originate from E_1f. This inconsistency can be also reflected in the comparison between the source rocks of K_2t and the natural gas in K_2t-E_1f, which indicates that K_2t-E_1f gas is not derived from the K_2t source rock.

The difference in $\delta^{13}C$ value between kerogen from Permian source rocks and ethane accords with the carbon isotopic fractionation demonstrated by Wu et al., 2020a, which shows a carbon-isotope affinity between kerogen and ethane from natural gas. It should be noted that the kerogens in the source rocks of P_3l and P_2g s are humic (Du et al., 2015; Zhang et al., 2018), while those of P_1q and P_3d are sapropelic (Cai et al., 2019; Ding et al., 2023). The natural gas in K_2t-E_1f is produced from sapropelic kerogens (as described above), indicating that it originates from sapropelic source rocks rather than humic source rock. The absence of genetic affinity between natural gas and source rocks of P_3l and P_2g precludes the possibility of gas supply from these source rocks. For P_3d, Du et al. (2020) found that the source rocks are mature in most parts of the lower Yangtze area and are in the dry gas window in the southwest. The thickness of P_3d is less than 50 m. The inconsistency between the calculated Ro value of oil-type gas and the maturity of source rocks shows that the contribution of the source rocks of P_3d is negligible, and the source of natural gas in this formation should be the underlying sapropelic source rock with higher maturity. In addition, while the carbonate rocks of P_2q may have hydrocarbon generation potential, their average TOC is only 0.26 % (Feng and Chen, 2007), which is below the generally accepted typical threshold of 0.5 % for carbonates serving as effective source rocks (Zhang et al., 2002). Moreover, the Devonian sandstone below the Cretaceous unconformity in Well A2 reveals a lack of carbonate rocks in P_2q. Presumably, the contribution of the carbonate rocks of P_2q to the natural gas in K_2t-E_1f gas is limited.

Maturity is an important determinant of the carbon isotopic characteristics of natural gas. The Ro values of natural gas in K_2t-E_1f were calculated using Eq. (2), with an average of 2.2 %. The source rocks of ϵ_1m were buried at depths greater than 6,000 m after the Cretaceous, reaching the thermal maturity level for dry gas generation. These source rocks are characterized by the cracking of C_2-C_5 gaseous hydrocarbons to methane and an increase in $\delta^{13}C_2$. Although natural gas shows high slope of $\delta^{13}C$ from methane to ethane (Fig. 6e), the maturity level of the source rocks of ϵ_1m determined through the reconstruction of burial and thermal evolution history is significantly higher than the calculated Ro values of natural gas. When the Ro of source rocks in ϵ_1m was 2.2 %, E_1f had not yet been formed. In this time, the Ro value of the source rocks of O_3w-S_1g is less than 1.6 %. When the source rocks of O_3w-S_1g were experiencing steady subsidence and sedimentation before the maximum burial depth was reached, they were in the main stage of liquid hydrocarbon cracking. Therefore, it is more likely that the natural gas originates from the source rocks of O_3w-S_1g rather than those of ϵ_1m, which is also evidenced by the similarities in carbon isotope and genetic type observed between the natural gas in K_2t-E_1f and the sapropelic source rocks of O_3w-S_1g.

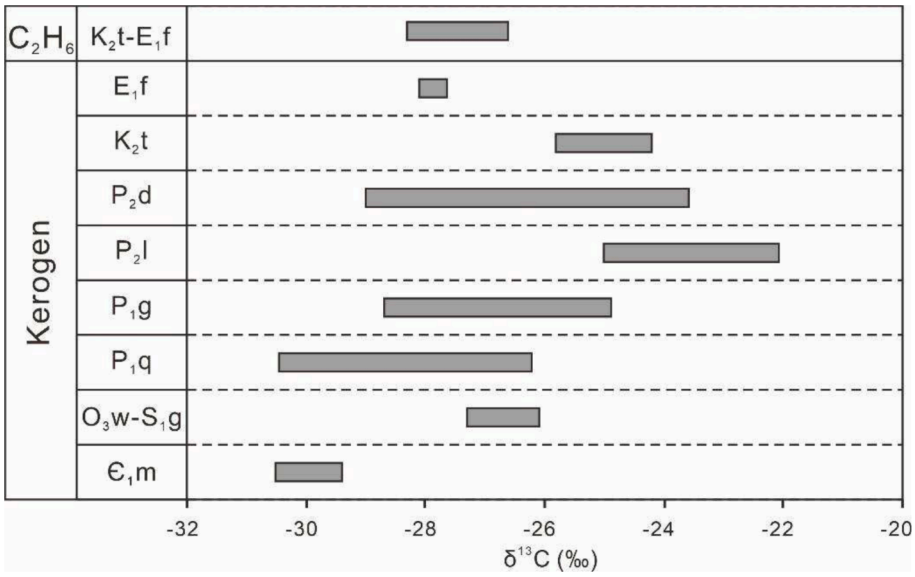

Fig. 8. Carbon isotope values of C_2H_6 in K_2t-E_1f gas in the Zhujiadun gas field and kerogen in potential , and Source rocks in the Yancheng Sag. The $\delta^{13}C$ values of kerogen have been obtained from Chen et al., 2008a, Feng and Chen, 2007, Zhao et al., 2021Zhao et al., 2023.

6. Conclusions

Genetic type, maturity and geochemistry characteristic of natural gas from the K_2t-E_1f were determined through organic geochemistry and gold-tube hydrous pyrolysis experiments. Integration of gold-tube hydrous pyrolysis experiments with basin modeling provides insights into the formation of gas pools in the Yancheng Sag.

As revealed in organic geochemistry analysis, it has been determined that the natural gas in K_2t-E_1f is an oil-type gas mainly originating from secondary cracking. Affected by thermal maturity, sharp increase appears in isotopic characteristics from methane to ethane.

The thermal maturation history reconstructed through basin modeling shows that the potential source rocks in the Yancheng Sag are post mature, and particularly, the Paleozoic source rocks are high mature or even over-mature.

Empirical equations suitable for calculating the maturity of natural gas in the study area were established according to the gold-tube hydrous pyrolysis experiments. Based on such calculation, the maturity levels of natural gas with $\delta^{13}C_1$ values ranging from −39.6 ‰ to −36.7 ‰ were evaluated. The calculated Ro values vary from 1.84 % to 2.46 %, with an average of 2.2 %, indicating that the natural gas in the Zhujiadun gas field is produced primarily from secondary cracking.

The affinity between potential source rocks and natural gas in terms of origin, maturity, and carbon isotopes indicates that the natural gas in the Zhujiadun gas field predominantly originates from the source rocks of the Ordovician Wufeng-Silurian Gaojianbian formations, with limited contributions from Carboniferous source rocks and the source rocks of the Cambrian Mufushan Formation.

CRediT authorship contribution statement

Yuantao Tang: Writing – original draft, Investigation. **Kai Xue:** Software, Data curation. **Xianzhi Gao:** Supervision, Methodology, Conceptualization. **Yan Song:** Writing – review & editing, Data curation. **Heyong Li:** Supervision. **Yonghui Wang:** Writing – review & editing, Data curation.

Declaration of competing interest

The authors declare that they have no known competing financial interests or personal relationships that could have appeared to influence the work reported in this paper.

Acknowledgements

We acknowledge two anonymous reviewers and the associate editor Dr. Tapan Chakraborty for their valuable comments and suggestions, which greatly improve the manuscript of an earlier version. This work is financially supported by the SINOPEC Jiangsu Oilfield Company -China University of Petroleum (Beijing) Cooperation Science and Technology Project (No. 31450008-22-ZC0607-0004). The authors sincerely thank the Research Institute of Exploration and Development of SINOPEC Jiangsu Oilfield Company for their support in sample collection and basic data.

Data availability

Data will be made available on request.

References

Behar, F., Vandenbroucke, M., Teermann, S.C., Hatcher, P.G., Leblond, C., Lerat, O., 1995. Experimental simulation of gas generation from coals and a marine kerogen. ChemGeol.Processes of Natural Gas Formation 126, 247–260. https://doi.org/10.1016/0009-2541(95)00121-2.

Bernard, B.B., Brooks, J.M., Sackett, W.M., 1978. Light hydrocarbons in recent Texas continental shelf and slope sediments. J. Geophys. Res. Oceans 83, 4053–4061. https://doi.org/10.1029/JC083iC08p04053.

Berner, U., Faber, E., 1996. Empirical carbon isotope/maturity relationships for gases from algal kerogens and terrigenous organic matter, based on dry, open-system pyrolysis. Organic Geochemistry, Proceedings of the 17th International Meeting on Organic Geochemistry 24, 947–955. doi: 10.1016/S0146-6380(96)00090-3.

Berner, U., Faber, E., 1988. Maturity related mixing model for methane, ethane and propane, based on carbon isotopes. In: Mattavelli, L., Novelli, L. (Eds.), Organic Geochemistry in Petroleum Exploration. Pergamon, Amsterdam, pp. 67–72, 10.1016/B978-0-08-037236-5.50012-9.

Berner, U., Faber, E., Scheeder, G., Panten, D., 1995. Primary cracking of algal and landplant kerogens: Kinetic models of isotope variations in methane, ethane and propane. Chemical Geology, Processes of Natural Gas Formation 126, 233–245. https://doi.org/10.1016/0009-2541(95)00120-4.

Cai, L., Xiao, G., Guo, X., Wang, J., Wu, Z., Li, B., 2019. Assessment of Mesozoic and Upper Paleozoic source rocks in the South Yellow Sea Basin based on the continuous borehole CSDP-2. Mar. Pet. Geol. 101, 30–42. https://doi.org/10.1016/j.marpetgeo.2018.11.028.

Chang, X., Liu, B., Zhang, J., Mao, F., 2004. Genetic mechanism of natural gas and condensate in Yancheng Sag. Mar. Geol. Quat. Geol. 95–100.

Chen, A., Song, N., Wang, W., 2008a. An evaluation of the source bed in Upper Cretaceous Taizhou Formation, Subei basin. China Offshore Oil and Gas 28–33.

Chen, A., Wang, W., Yue, K., Huang, J., 2001. Gas source of Zhujiadun gas field, Yancheng basin and its discovery significance. Pet. Explor. Dev. 45–49.
Chen, J., Ge, H., Chen, X., Deng, C., Liang, D., 2008b. Classification and origin of natural gases from Lishui Sag, the East China Sea Basin. Sci China Ser D Earth Sci 51, 122–130. https://doi.org/10.1007/s11430-008-5001-5.
Chen, J., Wang, X., Chen, J., Ni, Y., Xiang, B., Liao, F., He, W., Yao, L., Li, E., 2021. New equation to decipher the relationship between carbon isotopic composition of methane and maturity of gas source rocks. Sci. China Earth Sci. 64, 470–493. https://doi.org/10.1007/s11430-020-9692-1.
Chen, L., 2009. Estimation of the amount of erosion at unconformities in the last stage of the Eocene Sanduo period in the Subei Basin. China. Pet. Sci. 6, 383–388. https://doi.org/10.1007/s12182-009-0058-0.
Dai, J., Ni, Y., Gong, D., Huang, S., Liu, Q., Hong, F., Zhang, Y., 2024. Characteristics of carbon isotopic composition of alkane gas in large gas fields in China. Pet. Explor. Dev. 51, 251–261. https://doi.org/10.1016/S1876-3804(24)60021-2.
Dai, J., Ni, Y., Gong, D., Feng, Z., Liu, D., Peng, W., Han, W., 2017. Geochemical characteristics of gases from the largest tight sand gas field (Sulige) and shale gas field (Fuling) in China. Mar. Pet. Geol. 79, 426–438. https://doi.org/10.1016/j.marpetgeo.2016.10.021.
Dai, J., Qi, H., Song, Y., 1985. Primary discussion of some parameters for identification of coal-and oil-type gases. Acta Pet. Sin. 6, 31–38.
Dai, J., Song, Y., Dai, C., Wang, D., 1996. Geochemistry and Accumulation of Carbon Dioxide Gases in China. AAPG Bull. 80, 1615–1625. https://doi.org/10.1306/64EDA0D2-1724-11D7-8645000102C1865D.
Dai, J., Xia, X., Qin, S., Zhao, J., 2004. Origins of partially reversed alkane δ13C values for biogenic gases in China. Organic Geochemistry, Conference on Emerging Concepts in Organic Petrology and Geochemistry 35, 405–411. https://doi.org/10.1016/j.orggeochem.2004.01.006.
Dieckmann, V., Ondrak, R., Cramer, B., Horsfield, B., 2006. Deep basin gas: New insights from kinetic modelling and isotopic fractionation in deep-formed gas precursors. Mar. Pet. Geol. 23, 183–199. https://doi.org/10.1016/j.marpetgeo.2005.08.002.
Ding, J., Sun, J., Nie, H., Yang, X., Ye, Y., Shi, G., Wang, R., Huang, B., Li, H., 2023. Application of biomarkers in characterization of organic matter source, maturity and palaeoredox condition of black shales from the upper Permian Dalong Formation in Southern Anhui Province, South China. Geol. J. 58, 1741–1759. https://doi.org/10.1002/gj.4691.
Du, X., Song, X., Zhang, M., Lu, Y., Lu, Y., Chen, P., Liu, Z., Yang, S., 2015. Shale gas potential of the Lower Permian Gufeng Formation in the western area of the Lower Yangtze Platform, China. Mar. Pet. Geol. 67, 526–543. https://doi.org/10.1016/j.marpetgeo.2015.05.031.
Du, X., Lu, Y., Chen, P., Li, X., Song, X., 2020. The Lower Yangtze area: A next shale gas block for China? Preliminary potential assessment from some geology and organic geochemistry information. Geol. J. 55, 3157–3178. https://doi.org/10.1002/gj.3585.
Farouk, S., Arafat, M., Fagelnour, M.S., Al-Kahtany, K., Gentzis, T., 2024a. Petroleum system assessment of the Beni Suef Basin, Western Desert. Egypt. Journal of African Earth Sciences 217, 105345. https://doi.org/10.1016/j.jafrearsci.2024.105345.
Farouk, S., Saada, S.A., Fagelnour, M., Tawfik, A.Y., Arafat, M., El-Kahtany, K., 2024b. Geochemical evaluation and basin modelling of the Cretaceous succession in the Azhar Oil field, West Beni Suef Basin. Egypt. Geological Journal 59, 1949–1967. https://doi.org/10.1002/gj.4979.
Farouk, S., Saada, S.A., Fagelnour, M.S., Arafat, M., 2024c. Petrophysical and Gas Chromatographic Analysis Integration for Hydrocarbon Identifications in Cretaceous Reservoirs, Azhar Field, Beni Suef Basin. Egypt. Egyptian Journal of Petroleum 33. https://doi.org/10.62593/2090-2468.1018.
Feng, W., Chen, A., 2007. Characteristics of Permian source rock and analysis of gas source of Well XQ- 1 in Yancheng Sag, Subei Basin. Marine Origin Petroleum Geology 12, 25–32.
Gai, H., Tian, H., Cheng, P., Zhou, Q., Li, T., Wang, X., Xiao, X., 2019. Influence of retained bitumen in oil-prone shales on the chemical and carbon isotopic compositions of natural gases: Implications from pyrolysis experiments. Mar. Pet. Geol. 101, 148–161. https://doi.org/10.1016/j.marpetgeo.2018.11.048.
Gao, G., Yang, S., Zhang, W., Wang, Y., Gang, W., Lou, G., 2018. Organic geochemistry of the lacustrine shales from the Cretaceous Taizhou Formation in the Gaoyou Sag, Northern Jiangsu Basin. Mar. Pet. Geol. 89, 594–603. https://doi.org/10.1016/j.marpetgeo.2017.10.023.
Gong, L., Gao, X., Stow, D., Qu, F., Zhang, G., Liu, P., 2022. What continued after the mass extinction: insights from carbonate microfacies and biological evolution around the Permian–Triassic boundary in the middle Upper Yangtze Platform, SW China. Geol. Mag. 160, 35–59. https://doi.org/10.1017/S0016756822000632.
Hackley, P.C., Scott, C., Birdwell, J.E., Nedzweckas, J.L., Valentine, B.J., Zhang, T., Nesheim, T.O., 2024. Insights on Using Solid Bitumen Reflectance as a Thermal Maturity Proxy in the Bakken Formation, Williston Basin, USA. ACS Omega 9, 33983–33997. https://doi.org/10.1021/acsomega.4c04547.
He, K., Zhang, S., Mi, J., Zhang, W., 2018. The evolution of chemical groups and isotopic fractionation at different maturation stages during lignite pyrolysis. Fuel 211, 492–506. https://doi.org/10.1016/j.fuel.2017.09.085.
Hill, R.J., Tang, Y., Kaplan, I.R., 2003. Insights into oil cracking based on laboratory experiments. Org Geochem. 34, 1651–1672. https://doi.org/10.1016/S0146-6380(03)00173-6.
Hu, G., Li, J., Shan, X., Han, Z., 2010. The origin of natural gas and the hydrocarbon charging history of the Yulin gas field in the Ordos Basin, China. International Journal of Coal Geology, ICCP-TSOP 2008 Selected papers from the ICCP-TSOP joint meeting 2008: International conference on coal and organic petrology 81, 381–391. doi: 10.1016/j.coal.2009.07.016.
Hu, G., Li, J., Li, J., Li, Z., Luo, X., Sun, Q., Ma, C., 2008. Preliminary study on the origin identification of natural gas by the parameters of light hydrocarbon. Sci China Ser D Earth Sci 51, 131–139. https://doi.org/10.1007/s11430-008-5017-x.
Huang, S., Li, J., Wang, T., Jiang, Q., Jiang, H., Tao, X., Bai, B., Feng, Z., 2022. Application of Light Hydrocarbons in Natural Gas Geochemistry of Gas Fields in China. Annu. Rev. Earth Planet. Sci. 50, 13–53. https://doi.org/10.1146/annurev-earth-070921-054917.
James, A.T., 1990. Correlation of Reservoired Gases Using the Carbon Isotopic Compositions of Wet Gas Components (1). AAPG Bull. 74, 1441–1458.
James, A.T., Burns, B.J., 1984. Microbial Alteration of Subsurface Natural Gas Accumulations. AAPG Bull. 68, 957–960.
Korsch, R.J., Huazhao, M., Zhaocai, S., Gorter, J.D., 1991. The Sichuan basin, southwest China: a late proterozoic (Sinian) petroleum province. Precambrian Research, Proterozoic Petroleum 54, 45–63. https://doi.org/10.1016/0301-9268(91)90068-I.
Li, M., Chen, Z., Yi, S., Lin, S., Gao, Y., Huang, F., She, Y., Qiao, R., 2022. Origin and accumulation mechanisms of deep paleozoic oil and gas: A case study of the central Tarim basin, western China. J. Pet. Sci. Eng. 208, 109634. https://doi.org/10.1016/j.petrol.2021.109634.
Li, P., Hao, F., Guo, X., Zou, H., Yu, X., Wang, G., 2015. Processes involved in the origin and accumulation of hydrocarbon gases in the Yuanba gas field, Sichuan Basin, southwest China. Mar. Pet. Geol. 59, 150–165. https://doi.org/10.1016/j.marpetgeo.2014.08.003.
Li, P., Hao, F., Guo, X., Zou, H., Zhu, Y., Yu, X., Wang, G., 2016. Origin and distribution of hydrogen sulfide in the Yuanba gas field, Sichuan Basin, Southwest China. Mar. Pet. Geol. 75, 220–239. https://doi.org/10.1016/j.marpetgeo.2016.04.021.
Li, S., Liu, X., Cen, C., Yang, S., Xiao, E., Zhang, X., He, W., Liu, L., 2023. Sedimentary paleoenvironment and organic matter accumulation model of the Lower Silurian Gaojiabian Formation shales in the Lower Yangtze region. South China. Geoenergy Science and Engineering 221, 211347. https://doi.org/10.1016/j.geoen.2022.211347.
Li, Y., Chen, S., Wang, Y., Qiu, W., Su, K., He, Q., Xiao, Z., 2019. The origin and source of the Devonian natural gas in the Northwestern Sichuan Basin, SW China. J. Pet. Sci. Eng. 181, 106259. https://doi.org/10.1016/j.petrol.2019.106259.
Li, Y., Zhang, X., 2017. The whole story and significance of Zhujiadun Oilfields discovery. Journal of xi'an Shiyou University (social Science Edition) 26, 69–72.
Liang, C., Jiang, Z., Zhang, C., Guo, L., Yang, Y., Li, J., 2014. The shale characteristics and shale gas exploration prospects of the Lower Silurian Longmaxi shale, Sichuan Basin, South China. J. Nat. Gas Sci. Eng. 21, 636–648. https://doi.org/10.1016/j.jngse.2014.09.034.
Liang, J., Zhang, P., Chen, J., Gong, J., Yuan, Y., 2017. Hydrocarbon preservation conditions in Mesozoic–Paleozoic marine strata in the South Yellow Sea Basin. Nat. Gas Ind. B 4, 432–441. https://doi.org/10.1016/j.ngib.2017.05.013.
Liu, C., Jiang, Z., Zhou, X., Duan, Y., Lei, H., Wang, X., Atuquaye Quaye, J., 2021. Paleocene storm-related event beds in the Gaoyou Sag of the Subei Basin, eastern China: A new interpretation for these deep lacustrine sandstones. Mar. Pet. Geol. 124, 104850. https://doi.org/10.1016/j.marpetgeo.2020.104850.
Liu, Q., Wu, X., Wang, X., Jin, Z., Zhu, D., Meng, Q., Huang, S., Liu, J., Fu, Q., 2019. Carbon and hydrogen isotopes of methane, ethane, and propane: A review of genetic identification of natural gas. Earth Sci. Rev. 190, 247–272. https://doi.org/10.1016/j.earscirev.2018.11.017.
Lorant, F., Prinzhofer, A., Behar, F., Huc, A.-Y., 1998. Carbon isotopic and molecular constraints on the formation and the expulsion of thermogenic hydrocarbon gases. Chem. Geol. 147, 249–264. https://doi.org/10.1016/S0009-2541(98)00017-5.
Lotfy, N.M., Farouk, S., Hakimi, M.H., Ahmad, F., El Shennawy, T., El Nady, M.M., Salama, A., Shehata, A.M., 2024. Biomarker and isotopic characteristics of Miocene condensates and natural gases, West Delta deep marine concession, Eastern Mediterranean. Egypt. Sci Rep 14, 235. https://doi.org/10.1038/s41598-023-50418-4.
Lotfy, N.M., Qteishat, A., Farouk, S., Ahmad, F., Al-Kahtany, K., Hsu, C.S., 2022. Geochemical characteristics and genetic types of Ordovician tight gas in the Risha Gas Field, Eastern Jordan based on carbon and hydrogen isotope compositions. Mar. Pet. Geol. 143, 105810. https://doi.org/10.1016/j.marpetgeo.2022.105810.
Lu, S., Li, J., Xue, H., Chen, F., Xu, Q., Wang, M., Li, W., Pang, X., 2019. Pyrolytic Gaseous Hydrocarbon Generation and the Kinetics of Carbon Isotope Fractionation in Representative Model Compounds with Different Chemical Structures. Geochem. Geophys. Geosyst. 20, 1773–1793. https://doi.org/10.1029/2018GC007722.
Luo, Q., Goodarzi, F., Zhong, N., Qiu, N., Wang, X., Suchý, V., Khan, I., Zheng, X., Liu, B., Ardakani, O.H., Zhang, Y., Li, D., Wu, J., Fang, Z., Shi, R., Skovsted, C.B., Sanei, H., Xu, Y., Wu, J., Hu, W., Duan, G., 2025. Dispersed organic matter from pre-Devonian marine shales: A review on its composition, origin, evolution, and potential for hydrocarbon prospecting. Earth Sci. Rev. 261, 105027. https://doi.org/10.1016/j.earscirev.2024.105027.
Luo, Y., Liu, Y., Duan, H., 2020. Analysis on types and genesis of natural gas in Subei Basin. Complex Hydrocarbon Reservoirs 13, 22–27.
Ma, Y., Guo, X., Guo, T., Huang, R., Cai, X., Li, G., 2007. The Puguang gas field: New giant discovery in the mature Sichuan Basin, southwest China. AAPG Bull. 91, 627–643. https://doi.org/10.1306/11030606062.
Mastalerz, M., Drobniak, A., Stankiewicz, A.B., 2018. Origin, properties, and implications of solid bitumen in source-rock reservoirs: A review. Int. J. Coal Geol. 195, 14–36. https://doi.org/10.1016/j.coal.2018.05.013.
Odden, W., Patience, R.L., Van Graas, G.W., 1998. Application of light hydrocarbons (C_4–C_{13}) to oil/source rock correlations: a study of the light hydrocarbon compositions of source rocks and test fluids from offshore Mid-Norway. Org Geochem. 28, 823–847. https://doi.org/10.1016/S0146-6380(98)00039-4.

Peng, J., Liu, X., Pan, W., Li, H., Qiu, J., 2023. The source and formation characteristics of the Zhujiadun gas reservoirs in the Yancheng Sag. Subei Basin. Energy Geoscience 4, 100158. https://doi.org/10.1016/j.engeos.2023.100158.
Prinzhofer, A., Vega, M.A.G., Battani, A., Escudero, M., 2000. Gas geochemistry of the Macuspana Basin (Mexico): thermogenic accumulations in sediments impregnated by bacterial gas. Mar. Pet. Geol. 17, 1029–1040. https://doi.org/10.1016/S0264-8172(00)00033-7.
Quaye, J.A., Jiang, Z., Zhou, X., 2019. Bioturbation influence on reservoir rock quality: A case study of Well Bian-5 from the second member Paleocene Funing Formation in the Jinhu sag, Subei basin, China. J. Pet. Sci. Eng. 172, 1165–1173. https://doi.org/10.1016/j.petrol.2018.09.026.
Schmidt, J.S., Menezes, T.R., Souza, I.V.A.F., Spigolon, A.L.D., Pestilho, A.L.S., Coutinho, L.F.C., 2019. Comments on empirical conversion of solid bitumen reflectance for thermal maturity evaluation. Int. J. Coal Geol. 201, 44–50. https://doi.org/10.1016/j.coal.2018.11.012.
Schoell, M., 1983. Genetic Characterization of Natural Gases. AAPG Bull. 67, 2225–2238.
Schwangler, M., Harris, N.B., Waldron, J.W.F., 2020. Source rock characterization and oil-to-source rock correlation of a Cambrian -Ordovician fold-and-thrust belt petroleum system, western Newfoundland. Mar. Pet. Geol. 115, 104283. https://doi.org/10.1016/j.marpetgeo.2020.104283.
Shen, C., Yuan, H., Kuang, M., Zhang, X., Chen, C., Ye, Z., Yang, P., Li, Y., Xiao, Q., Wang, T., Wang, B., 2024. Sources of natural gas in the Middle-Permian carbonate succession in the central-northern Sichuan Basin, Southwest China. J. Asian Earth Sci. 268, 106164. https://doi.org/10.1016/j.jseaes.2024.106164.
Shuai, Y., Zou, Y., Peng, P., 2003. Kinetic model for the stable carbon isotope of methane: the state of the art. Advance in Earth Sciences 18, 405–411.
Stahl, W.J., 1977. Carbon and nitrogen isotopes in hydrocarbon research and exploration. Chem. Geol. 20, 121–149. https://doi.org/10.1016/0009-2541(77)90041-9.
Su, A., Chen, H., Feng, Y., Zhao, J., Nguyen, A.D., 2022. Multistage fracturing history in the Paleocene lacustrine shale oil reservoirs of the Subei Basin. Eastern China. Marine and Petroleum Geology 144, 105835. https://doi.org/10.1016/j.marpetgeo.2022.105835.
Sweeney, J.J., Burnham, A.K., 1990. Evaluation of a Simple Model of Vitrinite Reflectance Based on Chemical Kinetics1. AAPG Bull. 74, 1559–1570. https://doi.org/10.1306/0C9B251F-1710-11D7-8645000102C1865D.
Tang, Y., Perry, J.K., Jenden, P.D., Schoell, M., 2000. Mathematical modeling of stable carbon isotope ratios in natural gases††We dedicate this paper to Bill Sackett on the occasion of his 70th birthday. Geochim. Cosmochim. Acta 64, 2673–2687. https://doi.org/10.1016/S0016-7037(00)00377-X.
Tian, H., Xiao, X., Wilkins, R.W.T., Tang, Y., 2012. An experimental comparison of gas generation from three oil fractions: Implications for the chemical and stable carbon isotopic signatures of oil cracking gas. Org Geochem. 46, 96–112. https://doi.org/10.1016/j.orggeochem.2012.01.013.
Tissot, B.P., Welte, D.H., 1978. Formation of Petroleum in Relation to Geological Processes. Timing of Oil and Gas Generation. In: Tissot, B.P., Welte, D.H. (Eds.), Petroleum Formation and Occurrence: A New Approach to Oil and Gas Exploration. Springer, Berlin Heidelberg, Berlin, Heidelberg, pp. 185–201. https://doi.org/10.1007/978-3-642-96446-6_11.
Wang, M., Guo, Z., Jiao, C., Lu, S., Li, J., Xue, H., Li, J., Li, J., Chen, G., 2019. Exploration progress and geochemical features of lacustrine shale oils in China. J. Pet. Sci. Eng. 178, 975–986. https://doi.org/10.1016/j.petrol.2019.04.029.
Wang, Q., Lu, H., Greenwood, P., Shen, C., Liu, J., Peng, P., 2013. Gas evolution during kerogen pyrolysis of Estonian Kukersite shale in confined gold tube system. Org Geochem. 65, 74–82. https://doi.org/10.1016/j.orggeochem.2013.10.006.
Wu, J., Qi, W., Jiang, F.-J., Luo, Q.-Y., Zhang, C.-L., Hu, H.-Z., Wang, Z., Ma, Q.-S., Tang, Y.-C., 2021. Influence of sulfate on the generation of bitumen components from kerogen decomposition during catagenesis. Pet. Sci. 18, 1611–1618. https://doi.org/10.1016/j.petsci.2021.09.029.
Wu, X., Liu, Q., Chen, Y., Zhai, C., Ni, C., Yang, J., 2020a. Constraints of molecular and stable isotopic compositions on the origin of natural gas from Middle Triassic reservoirs in the Chuanxi large gas field, Sichuan Basin, SW China. J. Asian Earth Sci. 204, 104589. https://doi.org/10.1016/j.jseaes.2020.104589.
Wu, Z., He, S., Han, Y., Zhai, G., He, X., Zhou, Z., 2020b. Effect of Organic Matter Type and Maturity on Organic Matter Pore Formation of Transitional Facies Shales: A Case Study on Upper Permian Longtan and Dalong Shales in Middle Yangtze Region. China. J. Earth Sci. 31, 368–384. https://doi.org/10.1007/s12583-019-1237-6.
Wygrala, B., 1989. Integrated Study of an Oil field in the Southern Po Basin, Northern Italy. Kernforschungsanlage Jülich GmbH, Zentralbiliothek, Verlag, Jülich, Berichte der Kernforschungsanlage Jülich.
Xiong, Y., Zhang, H., Geng, X., Geng, A., 2004. N-octadecane pyrolysis and its geochemical significance. Chin. Sci. Bull. 49, 72–75.
Xu, Z., 2002. New evidences for natural gas source of Zhujiadun Gasfield. Geol. J. China Univ. 423–428.
Yuan, Y., Yu, H., Li, T., Li, S., 2016. Mesozoic tectonothermal events in centra Lower Yangtze area and impacts on hydrocarbon generation of marine source rocks. Chin. J. Geophys. 06, 2191–2202.
Zhang, H., Qian, Q., Chen, Y., Huang, Z., 2006. Discussion on natural gas source rocks in Yancheng Sag, Subei Basin. Journal of Oil and Gas Technology 7–9.
Zhang, H., Xiong, Y., Liu, J., Liao, Y., Geng, A., 2005. Pyrolysis kinetics of pure n-C18H38 (I): gaseous hydrocarbon and carbon isotope evolution. Acta Geol. Sin. 79, 569–574.
Zhang, J., Li, X., Zhang, X., Zhang, M., Cong, G., Zhang, G., Wang, F., 2018. Geochemical and geological characterization of marine–continental transitional shales from Longtan Formation in Yangtze area, South China. Mar. Pet. Geol. 96, 1–15. https://doi.org/10.1016/j.marpetgeo.2018.05.020.
Zhang, S., Liang, D., Zhang, D., 2002. Evaluation criteria for Paleozoic effective hydrocarbon source rocks. Pet. Explor. Dev. 29, 8–12.
Zhao, Q., Wang, J., Chen, J., Zhao, Y., Dong, H., Zhang, Y., Liang, J., 2021. Optimization of evaluation index of Paleozoic high mature marine source rock in the Lower Yangze region. Geol. Bull. China 40, 330–340.
Zhao, Q., Xie, D., Chen, J., Liang, J., Zhang, Y., Wang, J., Dong, H., Yuan, Y., 2023. Evaluation and biocenetic derivation and sedimentary environment of source rocks from Permian in the Lower Yangze region. Geol. Bull. China 42, 1154–1165.
Zhu, H., Meng, X., 2004. Analyzing the characteristics of petroleum system in Yancheng Sag. Nat. Gas Ind. 18–21.
Zou, C., Dong, D., Wang, S., Li, J., Li, X., Wang, Y., Li, D., Cheng, K., 2010. Geological characteristics and resource potential of shale gas in China. Pet. Explor. Dev. 37, 641–653. https://doi.org/10.1016/S1876-3804(11)60001-3.

Further reading

Li, J., Li, Z., Wang, X., Wang, D., Xie, Z., Jin, L.i., Wang, Y., Han, Z., Ma, C., Wang, Z., Cui, H., Wang, R., Hao, A., 2017. New indexes and charts for genesis identification of multiple natural gases. Pet. Explor. Dev. 44, 535–543. https://doi.org/10.1016/S1876-3804(17)30062-9.